ELSEVIER

Materials Science and Engineering B74 (2000) 56–60

MATERIALS SCIENCE & ENGINEERING B

www.elsevier.com/locate/mseb

GaAs homojunction interfacial workfunction internal photoemission (HIWIP) far-infrared detectors

A.G.U. Perera [a,*], W.Z. Shen [a], H.C. Liu [b], M. Buchanan [b], W.J. Schaff [c]

[a] *Department of Physics and Astronomy, Georgia State University, Atlanta, GA 30303, USA*
[b] *Institute for Microstructural Sciences, National Research Council, Ottawa, Ont., Canada K1A OR6*
[c] *School of Electrical Engineering, Cornell University, Ithaca, NY 14853, USA*

Abstract

The recent development of p-GaAs homojunction interfacial workfunction internal photoemission (HIWIP) far-infrared (>40 μm) detectors is briefly reviewed. The emphasis is on the detector performance, which includes responsivity, quantum efficiency, bias effects, cut-off wavelength, uniformity, noise, and negative capacitance characteristics. Promising results indicate that p-GaAs HIWIP detectors have great potential to become a strong competitor in far-infrared applications. © 2000 Elsevier Science S.A. All rights reserved.

Keywords: GaAs; Homojunction interfacial workfunction internal photoemission (HIWIP); Far-infrared detectors

1. Introduction

The far-infrared (FIR) range is the source of much of the astrophysics information, such as dust radiation, molecular and atomic emission lines associated with important species C, O, and H_2O. Therefore, high performance FIR detectors as well as large focal plane arrays are in very high demand for space astronomy applications [1], such as NASA's Stratospheric Observatory for Infrared Astronomy (SOFIA), airborne mission, Next Generation Space Telescope (NGST), and ESA's Far-infrared and Sub-mm Telescope (FIRST) programs, for studying interacting galaxies, star formation and composition, and interstellar clouds. Although stressed Ge:Ga detectors respond [2] up to ~ 220 μm, there are many technological challenges for fabricating larger format arrays in germanium [3]. Recently, homojunction workfunction internal photoemission (HIWIP) FIR detectors were proposed using thin, highly doped emitter layer and undoped intrinsic layer structures [4], which opens new options for developing FIR imaging devices by taking advantage of the mature and uniform Si and GaAs material growth and monolithic integration technology. This paper reports the performance of p-GaAs HIWIP FIR detector with the emphasis on responsivity (quantum efficiency), defectivity, cut-off wavelength, uniformity, noise, and negative capacitance characteristics.

The sample 9604 was grown by molecular beam epitaxy (MBE) with substrate temperature at 560°C. The MBE epilayers consist of a 3000-Å bottom contact (p^{++}) layer, a 1500-Å undoped (i) layer, 20 periods of thin emitter (p^{+}) layers (thickness 150 Å) and undoped i layers (thickness 800 Å), and finally a 3000-Å top emitter layer and a 3000-Å top contact layer. The emitter layers were doped with Be to 4×10^{18} cm^{-3} near the Mott transition value [4]. The top and bottom contact layers were doped to $2–3 \times 10^{19}$ cm^{-3}, far above the Mott transition value to ensure an ohmic contact. Fig. 1 shows the schematic of the detector after device processing and the energy-band diagram. Secondary ion mass spectroscopy (SIMS) measurements confirmed the doping levels and profile. The contact was formed by deposition of Ti–Pt–Au.

2. Spectral response and quantum efficiency

The responsivity (R) spectra of the p-GaAs HIWIP FIR detector (mesa area 400×400 μm, optical window area 260×260 μm) under different forward biases at

* Corresponding author. Fax: +1-404-6511427.
E-mail address: uperera@gsu.edu (A.G.U. Perera)

PII: S0921-5107(99)00534-6

4.2 K are shown in Fig. 2(a). These responsivity curves show a strong bias dependence, and increase significantly with increasing bias. However, the bias cannot be increased indefinitely because of the increase in dark current. The highest responsivity obtained here is 3.10 ± 0.05 A/W at a bias of 192.0 mV. Fig. 2(b) shows the bias dependences of the defectivity (D^*) and peak quantum efficiency (η_p) determined from $R_p = q\lambda_p\eta_p/hc$, where q is the elementary charge, λ_p is the peak wavelength, h is the Planck constant, and c is the speed of light in vacuum. The quantum efficiency (η) (responsivity) is roughly linear under low biases and gradually saturates at high biases. The defectivity is almost independent of the applied bias and the maximum defectivity occurs at a bias just below the value at which η (responsivity) saturates, as in the case of quantum well infrared photodetectors (QWIPs) [5]. At high biases, the dark current increases rapidly thereby reducing D^*. At low biases, the barrier collection efficiency η_c decreases, lowering D^*. The highest defectivity observed was 5.9×10^{10} cm $\sqrt{\text{Hz}}$/W at 4.2 K under a bias of 83.0 mV.

The maximum quantum efficiency (η_{max}) in HIWIP FIR detectors can be estimated by taking the free carrier absorption and inelastic scattering loss into account. By assuming a constant inelastic scattering mean free path L_z and a constant absorption coefficient (α_p) in an emitter layer of thickness d with $2(N+1)$ optical passes due to multilayer (N) structures (1 comes from an additional stacked layer), η_{max} is given by:

$$\eta_{max} = \{1 - \exp[-2(N+1)\alpha_p d]\} \exp\left(-\frac{d}{L_z}\right)$$

$$\approx 2(N+1)\alpha_p d \cdot \exp\left(-\frac{d}{L_z}\right) \quad (1)$$

Using the concentration (P) dependence of the absorption coefficient in Ref. [6], i.e. $\alpha_p = 8.28 \times 10^{-16}$ cm$^2 \times P$ ($P = 4 \times 10^{18}$ cm^{-3}), 20 multilayers ($N = 20$), a typical value of $L_z \approx 200 \sim 300$ Å in p-GaAs [7], and an emitter layer thickness of 150 Å, given $\eta_{max} = 12.7\%$, which is in good agreement with the experimental result of 12.5% at a bias of 192.0 mV.

The bias behavior of η in Fig. 2(b) results from the fact that the net quantum efficiency has two components. One is η_{max} as discussed above (including both the photon absorption probability and internal quantum efficiency), and the other is the barrier collection efficiency (η_c), which is bias dependent due to the image force effect [4]:

$$\eta_c \propto \exp\left(-\frac{x_m}{L_s}\right) \quad (2)$$

where the distance from the interface to the barrier maximum $x_m = \sqrt{q/16\pi\varepsilon_0\varepsilon_s F}$, where F is the electric field in the i region, and L_s the hole scattering length in the i region. A semi-log plot of η_c as a function of x_m is shown in the inset of Fig. 1(b). The linear relation demonstrates that the experimental results can be well described by the above simple approximation. The solid line in the figure corresponds to the regression of the experimental data, which yields the hole scattering length L_s of 276 ± 2 Å in p-GaAs.

The responsivity curves shown in Fig. 3(a) also display a strong bias dependence of cut-off wavelength (λ_c), increasing with the applied bias due to the image force effect. The experimental data are shown as solid circles in Fig. 3(a). The theoretical model should include both the band edge lowering (ΔE_{maj}) due to high doping and the image force barrier lowering [4,6]:

$$\Delta = \dot{\Delta}E_{maj} - E'_F - \sqrt{\frac{qF}{4\pi\varepsilon_0\varepsilon_s}} \quad (3)$$

where ΔE_{maj} can be described by high density theory, $E'_F = E_F - 5 \pm 1$ (meV) is the modified Fermi level [6], and the last term is the bias dependent barrier lowering ($\Delta\Phi$). The λ_c is then calculated by λ_c (μm) $= 1.24/\Delta$ (eV). Using the parameters for p-GaAs given in Ref. [4] and the detector structure parameters, the theoretical results are shown in Fig. 3(a) by the solid curve. It is seen that the experimental λ_c is in good agreement with the calculation: the maximum deviation between the theory and experiment is 1.0 meV. The cut-off wave-

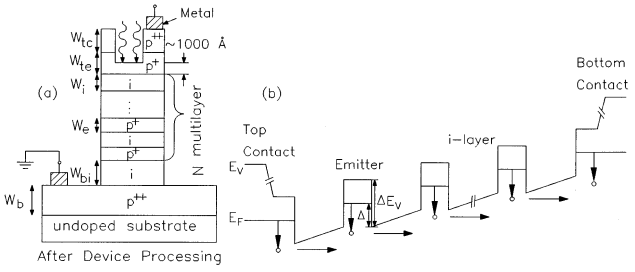

Fig. 1. (a) Schematic of the multilayer p-GaAs HIWIP detectors after device processing. p^{++}, p^+ and i are the contact layer, emitter layer and undoped layer, respectively. A window is opened on the top side for frontside illumination. (b) Energy-band diagram of the detectors under forward bias.

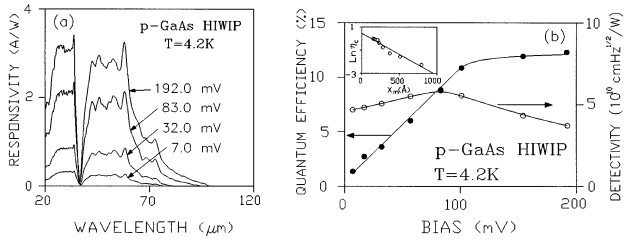

Fig. 2. (a) Spectral response of p-GaAs HIWIP FIR detector measured at a resolution of 4.0 cm^{-1} and temperature of 4.2 K under different forward bias values. The deep valley at 36.5 μm is due to the transverse optical (TO) phonons of GaAs. (b) Bias dependences of peak quantum efficiency measured at 30.0 μm (filled circles) and device defectivity (open circles).

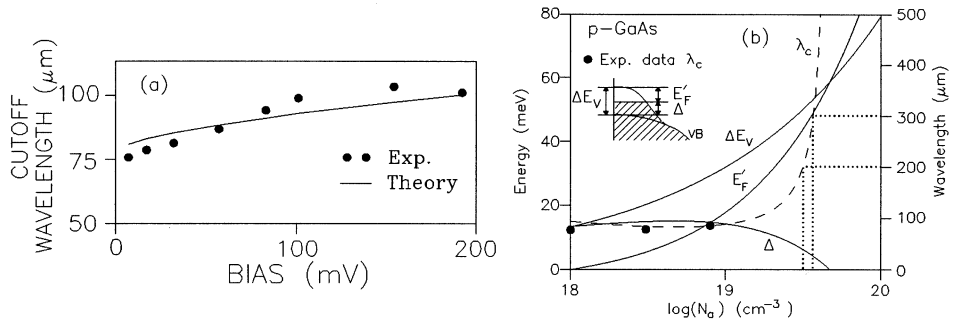

Fig. 3. (a) Bias dependence of cut-off wavelength in the p-GaAs HIWIP detector at 4.2 K. The maximum deviation between the theory (solid curve) and experiment (filled circles) is 1.0 meV. (b) Calculated doping concentration (N_a) dependence of the shift for the valence band edge ΔE_v, interfacial workfunction Δ, and λ_c at zero bias from the high density theory for p-GaAs. The experimental λ_c obtained from p-GaAs HIWIP detectors are shown by solid circles. The dotted lines indicate concentration (3.2×10^{19} and 3.6×10^{19} cm^{-3}) needed to obtain $\lambda_c = 200$ and 300 μm, respectively, at low bias.

length is tunable by applied voltage (from 80 to 100 μm), and can also be tailored through the emitter layer doping concentration as shown in Fig. 3(b).

3. Dark current and noise

The dark current of seven randomly chosen relatively large mesas (mesa area 600×600 μm, optical window area 460×460 μm) at 4.2 K was quite uniform (see inset of Fig. 4) with a standard deviation of 15.4% at a bias voltage of 200 mV. Furthermore, the bias dependence of D^* for the seven mesas is shown in Fig. 4, the values are within experimental errors. The relatively low D^* here is due to some dark current leakage in larger mesas. These results clearly demonstrate the possibility of high uniformity required for large FIR focal plane arrays, since the typical pixel size for arrays is much smaller than the tested devices (e.g. 50×50 μm in GaAs/AlGaAs QWIPs [5]), and thus the dark current per pixel, together with the standard deviation, would be about two orders of magnitude smaller.

Typical current noise spectra of the studied p-GaAs HIWIP FIR detector at 4.2 K for various forward bias values are presented in Fig. 5(a). Similar noise behavior was observed under reverse bias conditions. All the spectra display $1/f$ noise dependence at frequencies (f) below 1 kHz and are independent of frequency at higher values. The observed current noise spectra result from $1/f$ flicker noise and shot noise spectra. Absence of Lorentzian type noise in the noise spectra indicates that the current noise power density can be written as:

$$S_i(f) = C^{\mathrm{I}} \frac{I_{\mathrm{d}}^{\alpha}}{f^{\beta}} + C^{\mathrm{II}}, \tag{4}$$

where C^{I} is the amplitude of the flicker ($1/f$) noise, and $C^{\mathrm{II}} = 4qI_{\mathrm{d}}g$ denotes the shot noise spectrum, as in QWIPs [5], with I_{d} as the detector forward dark current and g as noise gain of the detector.

At low frequencies ($f \leq 1$ kHz), the value of β is found to vary from 1.0 to 1.2 and no simple relationship was found between β and bias. In order to understand the origin of the $1/f$ noise, a plot of $1/f$ noise power density (S_i) as a function of dark current I_{d} at

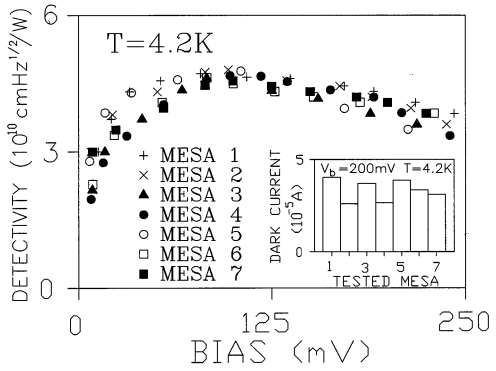

Fig. 4. Bias dependence of device defectivity in seven randomly chosen 460 μm-square mesas at temperature of 4.2 K. Shown in the inset is the dark current of the seven mesas at 4.2 K and a forward bias of 200 mV. Some dark current leakage is observed in these larger mesas. The uniformity of the p-GaAs HIWIP FIR detector is demonstrated by both the uniform dark current and defectivity.

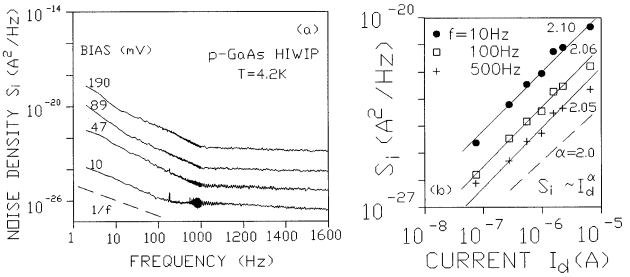

Fig. 5. (a) Measured dark current noise spectra of p-GaAs HIWIP far-infrared detector at 4.2 K for various forward biases. The dashed line represents the $1/f$ dependence of the noise power density S_i. (b) $1/f$ noise power density S_i as a function of the dark current I_{d} at frequencies of 10, 100 and 500 Hz. The dashed line represents the I_{d}^2 dependence of the noise power density S_i.

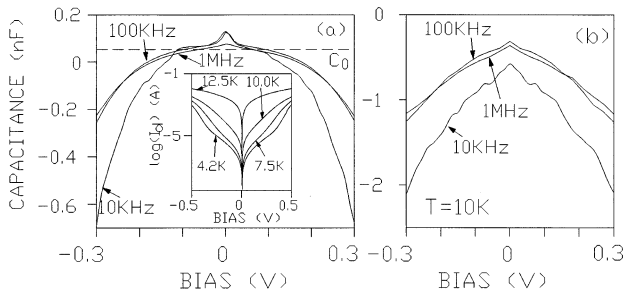

Fig. 6. Capacitance-bias characteristics measured at 10 kHz, 100 kHz, and 1 MHz for a p-GaAs HIWIP FIR detector at (a) 4.2 K and (b) 10.0 K. The horizontal dashed line in (a) indicates the value of the detector's geometrical capacitance C_0. Shown in the inset of (a) is the temperature dependence of the dark current.

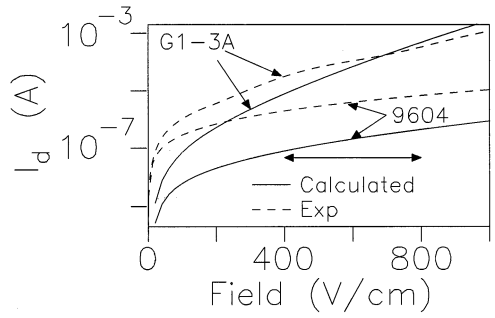

Fig. 7. The experimental dark current at 4.2 K for samples 9604 and G1-3A (dashed curves) converted to mesa area of 1×10^{-3} cm^2. The solid curves are the calculated dark current with a hole scattering length of 300 Å. The arrows indicate the detector operating bias range.

frequencies of 10, 100, and 500 Hz is measured and shown in Fig. 5(b). It is found that the $1/f$ noise power density is proportional to I_d^{α} with an α value of $2.05 \sim 2.10$. This type of behavior indicates that the origin of the $1/f$ noise could be interpreted in terms of a random fluctuation in the occupancy of the interface trap centers which can lead to generation-recombination (G-R) $1/f$ noise [8]. The free carrier absorption and internal photoemission in HIWIP detectors lead to carrier number fluctuations, which would result in current fluctuations in the external circuit when a net current flows through the detector. This kind of noise is related to the presence of interface localized states [8]. The interface states N_{is} has been estimated [9] in the order of 10^{11} cm^{-2}, a value which compared favorably with the density of interface states (2.5×10^{11} cm^{-2}) reported for MBE grown Be-doped p-type GaAs [10].

For frequencies above 1 kHz, the noise was independent of frequency and was dominated by shot noise. The noise gain is determined to be ~ 0.95, also in good agreement with the estimation of 0.984, obtained by combining the above experimental responsivity and quantum efficiency. The measured shot noise data can also be used to directly estimate the noise equivalent power (NEP) in the p-GaAs HIWIP FIR detector via $\mathrm{NEP} = \sqrt{S_i}/R$, where R is the responsivity. At a bias of 89 mV, the measured shot noise S_i is 8.3×10^{-25} A^2/Hz, and the responsivity of the detector at that bias is 2.12 A/W. This yields a NEP of 4.3×10^{-13} W/$\sqrt{\mathrm{Hz}}$ (defectivity D^* of 6.0×10^{10} cm $\sqrt{\mathrm{Hz}}$/W), also in good agreement with the above optical estimation D^* of 5.9×10^{10} cm$\sqrt{\mathrm{Hz}}$/W at a bias of 83 mV.

4. Negative capacitance

Typical capacitance-voltage characteristics of the p-GaAs HIWIP FIR detector at 4.2 and 10.0 K at different frequencies are presented in Fig. 6. The capacitance displays a maximum at zero bias, decreases rapidly with increasing bias voltage, and reaches negative values at higher biases. The decrease is more rapid at low frequencies. The capacitance at zero bias decreases with frequency, approaching the value of the geometrical capacitance ($C_0 = 44$ pF for the 800×800-μm mesa, see dashed line in Fig. 6(a)) at high frequencies. The p-GaAs HIWIP FIR detectors display a strong negative capacitance phenomenon in a wide range of frequency and bias. Unlike in other devices, even up to 1 MHz in HIWIP, the negative capacitance value keeps increasing with frequency, giving a stronger effect.

A fitting model [11] based on charging-discharging current and the inertial conducting current model shows good agreement with the experimental observations. The origin of this effect is believed to be due to the carrier capture and emission at interface states. In the presence of an AC perturbation with a small voltage δV, the interface traps can retain a sufficient quantity of charge so that they build a dipole layer which modulates the barrier height. Hence, the dark current and the conductance are also modified. The variation of barrier height δV_i arises mainly from carrier capture and emission at interface states. This process requires a certain period of time, which makes δV_i (and dark current) lag behind δV. The experimental test of a circuit combining the HIWIP structure with an external capacitance (~ 300 pF) in parallel shows that the circuit capacitance can be significantly reduced in a wide range of frequencies. Therefore, for FIR detection, the circuit incorporating the HIWIP detector can obviously use the negative capacitance to its advantage by decreasing its response time, since the response time is mainly determined by the circuit's RC constant. In addition, for any other focal plane array situations where low temperature is not an issue, this structure can be used to reduce the capacitance over a wide frequency range.

The effort to reduce the interface states in HIWIP detectors has made some progress. Fig. 7 shows the

experimental (dashed curve) and calculated (solid curves) dark currents at 4.2 K under positive biases for the above studied sample 9604 and another sample G1-3A (with doping concentration of 2.0×10^{19} cm^{-3}) converted to same device area of 1×10^{-3} cm^2. The thermionic field emission (TFE) current was found to be the major source of dark current in the p-GaAs HIWIP detectors at 4.2 K [6], so that increase in dark current with increased doping is expected as a result of modification to the Fermi-Dirac distribution. However, the dark current observed in 9604 sample was much higher than the values predicted according to the model. This has been attributed to the existence of interface defect states [6]. The existence of interface defect states can result in recombination via the defect states and generate currents. The G1-3A sample shows much better dark current results due to the quality of material, which is also supported by its lower noise characteristics. A plot R_0A (R_0 is dynamic resistance, A is device area) versus A for the 9604 sample showed a sharp drop indicating leakage, while in contrast, the G1-3A sample showed much improved almost constant R_0A values indicating much better quality material. Further evidence of this leakage can be seen from the relation of the dark current with the mesa area. The 9604 sample displayed a superlinear (slope = 1.62) increase with the mesa area, while the G1-3A displayed almost linear relation (slope = 0.95).

5. Conclusions

It is clear that higher performance and longer λ_c (~ 200 μm) p-GaAs HIWIP FIR detectors can be obtained [6] with the emitter layer concentration in the order of 10^{19} cm^{-3}. The type I Si HIWIP detector concept was also experimentally demonstrated using MBE grown Si p^+-i multilayer structure [12]. Further work is under way to design and fabricate high doping concentration type II Si HIWIP FIR detectors and longer λ_c (~ 200 μm) GaAs detectors. It is also possible to design detectors with wider wavelength ranges or to have multicolor detectors by changing the adjacent emitter layer doping concentrations.

Acknowledgements

This work was supported in part by the National Aeronautics and Space Administration under contract No. NAG 5-4950. The authors would like to acknowledge Dr S.G. Matsik at GSU for his technical help.

References

[1] M.W. Werner, M. Bothwell, The SIRTF Mission, Advances in Space Research 13 (1993) 521.
[2] N.M. Haegel, Nuclear Instructures Methods Phys. Res. A377 (1996) 501.
[3] E.E. Haller, Infrared Phys. 35 (1994) 127.
[4] A.G.U. Perera, H.X. Yuan, M.H. Francombe, J. Appl. Phys. 77 (1995) 915.
[5] B.F. Levine, J. Appl. Phys. 74 (1993) R1.
[6] W.Z. Shen, A.G.U. Perera, M.H. Francombe, H.C. Liu, M. Buchanan, W.J. Schaff, IEEE Trans. Electron Devices 45 (1998) 1671.
[7] J. Maserjian, Proc. SPIE 154O (1991) 127.
[8] O. Jantsch, IEEE Trans. Electron Devices 34 (1987) 1100.
[9] W.Z. Shen, A.G.U. Perera, IEEE Trans. Electron Devices 46 (1999) 811.
[10] J. Qiu, Q.D. Qian, R.L. Gunshor, M. Kobayashi, D.R. Menke, D. Li, N. Otsuka, Appl. Phys. Lett. 56 (1990) 1272.
[11] A.G.U. Perera, W.Z. Shen, M. Ershov, H.C. Liu, M. Buchanan, W.J. Schaff, Appl. Phys. Lett. 74 (1999) 3167.
[12] A.G.U. Perera, W.Z. Shen, H.C. Liu, M. Buchanan, M.O. Tanner, K.L. Wang, Appl. Phys. Lett. 72 (1998) 2307.